 doi:10.20944/preprints201906.0168.v1

Article

Reconfiguration of the pattern and transmission spectrum in near infrared band by plasmon nano-optical antenna

Dong-zhou Zhong [2]*,Hua Yang,Neng Zeng, Guang-Ze Yang and Jun-long Zhou [1]*

Faculty of Intelligent Manufacturing, Wuyi University, Jiangmen, Guangdong 529020,China.

* Correspondence:[1]*zhoujrkld88@126.com; [2]*dream_yu2002@126.com;

Abstract: We propose a novel plasmon nano-optical antenna that consists of three vertically superimposed discs with different materials. Two symmetrical nanometer-scale Yagi antenna elements with gold-material are embedded into the surface of the middle disc with silicon dioxide. Based on plasmon theory and Yagi antenna principle, we explore the properties of the far-field radiation and near-field transmission of the antenna in near infrared band. It is found that the pattern of the xoy plane in the antenna can be adjusted in arbitrary direction. The far-field pattern and near-field transmission spectrum can be reconfigured by changing the angle α of the Yagi antenna elements in the middle disc. Moreover, we also discuss the influences of the widths and lengths of the elements on the near-field transmission spectrum when α is fixed at 0 degree.

Keywords: Optical antenna; Radiation pattern; Transmission spectrum; Reconfiguration

1. Introduction

With the development of modern wireless communication system towards large capacity, multi-function and ultra-wide band, the performances of antennas need to be further improved. Reconfigurable antennas have great potential of the improvement of the performances. In recent years, they have attracted considered attentions due to their many advantages such as small size, versatility and easy to achieve diversity. Their working frequency, polarization and beam pointing or pattern may be varied by dynamically adjusting the structure and size. Some reconfigurable antennas operating in different frequency ranges have been proposed in recent works. For example, in microwave band, the working frequency[1,2],radiation pattern[3,4],and the polarization mode[5,6]can be reconstructed since the radiation-unit structure of the antenna is changed by using microelectronic and PIN diode switches. The working frequency and pattern of the antenna operating in terahertz frequency range can be reconfigured by varying the conductivity of graphene materials [7–10].

It is worth noting that plasmon nano-optical antennas (PNOAs) have attracted considerable interests since they have potential applications in many fields, such as the manipulation of the interaction between light and matter at nanoscale[11,12], optical scattering, redirecting incident light[13], photoelectric detection[14],sensing[15], heat transfer[16], spectroscopy[17,18] and so on. It is extremely attractive that the working frequency, polarization and pattern of the PNOA operating in near infrared band can be reconfigured by varying the size, shape, material and other factors. Recently, several reconfigurable PNOAs have been implemented experimentally and theoretically. For example, in 2013, J. Munarriz *et al*. designed a type of PNOA, in which the pattern can be manipulated by changing the incident angle and polarization mode of the excitation source[19].In 2016, Kai Chen and his co-workers proposed the PNOA that can be adjusted electromechanically. The optical properties of the antenna can be dynamically controlled by changing the gap width between

Preprints (www.preprints.org) | NOT PEER-REVIEWED | Posted: 18 June 2019 doi:10.20944/preprints201906.0168.v1

two suspended wires. The inverse adjustments of the resonance and electromagnetic enhancement can be implemented in the antenna[20]. Recently, metal nitride materials, such as TiN, ZrN, HfN and so on, have been applied in designing PNOA since they are both plasmonic and refractory. However, the near-field enhancement efficiency of metal nitrides shows lower than that of noble metals such as Au and Ag[21]. The optimum efficiency of the near-field enhancement can be obtained for small spherical nanoparticles with metal nitride material, but the efficiency is no more than 60%. Moreover, the enlargements or asymmetry of nitrides nanoparticle will reduce the efficiency[21].Therefore, many works about the PNOAs reported previously focuses on noble metals. However, in these works, the reconfiguration of the radiation pattern is only realized in some angle, and the beam pointing is very difficult to adjust arbitrarily. In this paper, we design a novel PNOA (see Fig.1), where the radiation and beam pointing can be easily adjusted by changing the angle α of the Yagi antenna elements in the middle disc. Moreover, we explore the properties of the far-field radiation and nea-field transmission.

2. Design procedure

In the far field, the normalized pattern function of the antenna can be expressed as

$$F(\theta,\varphi) = \frac{E(\theta,\varphi)}{E_m(\theta,\varphi)}, \tag{1}$$

where E (θ, φ) is the electric field amplitude; E_m (θ, φ) is the maximum value of E (θ, φ), where θ and φ are the zenith angle and the azimuth one in spherical coordinate system, respectively.

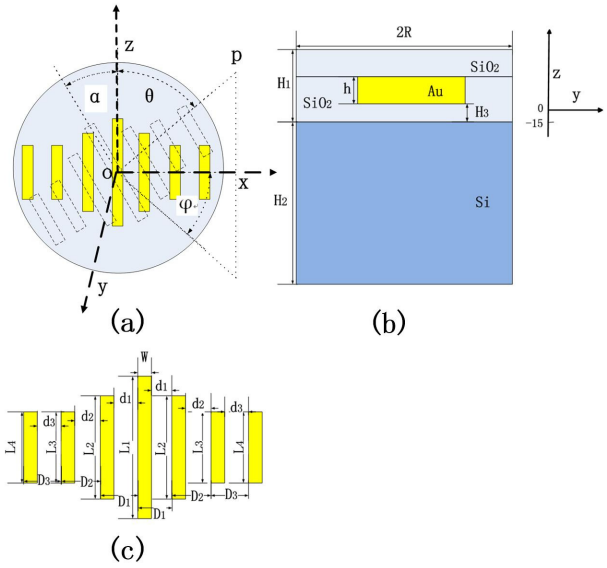

Figure 1. Schematic diagram of the plasmon nano-optical antenna, where (**a**) :the vertical view; (**b**): the side view;(**c**):the structure of the gold nano-block elements.

The directivity of the antenna is written as

$$D(\theta,\varphi) = \frac{U(\theta,\varphi)}{U_{ave}}, \tag{2}$$

where U(θ,φ) is the radiation intensity of the antenna; U_{ave} is the average radiation intensity. Eq.(2) is rewritten as

$$D(\theta,\varphi) = \frac{4\pi F^2(\theta,\varphi)}{\int_0^{2\pi}\int_0^{2\pi} F^2(\theta,\varphi) sin\theta\, d\theta\, d\varphi}. \tag{3}$$

As shown in Fig. 1, the PNOA consists of three vertically stacked discs. Here, the top and bottom discs are filled with silicon dioxide and silicon respectively, the middle disc is filled with silicon dioxide.

 doi:10.20944/preprints201906.0168.v1

A gold nano-block (GNB) is considered as an element of two symmetrical Yagi antennas embedded into the surface of the middle disc. The radius of all three discs are defined as R and set as 1200nm. The heights of the top and middle disks are defined as H_1 and set as 90nm. The height of the bottom disk is defined as H_2 and fixed at 200nm. The distance between the bottom surface of the Yagi antennas and the surface of the bottom disk is defined as H_3 and fixed at 20nm. The heights of all elements are defined as h and considered as 30nm. The lengths of the four elements of each Yagi antenna, in turn, are set as L_1, L_2, L_3 and L_4. d_j (j=1, 2, 3, the same below) is the distance between the jth and (j+1)th elements in each Yagi antenna. The weights of all four elements in each Yagi antenna are defined as w and set as 30nm. In addition, the middle disc with two symmetrical Yagi antennas is dextro oriented.

According to the design principle of traditional Yagi antenna given in [22], we have

$$L_1 = 0.55b_0, L_2 = 0.45b_0, L_3 = L_4 = 0.3b_0 \tag{4}$$

$$d_1 = 0.55b_1, d_2 = d_3 = 0.3b_2 \tag{5}$$

where b_0 and b_1 are constant. Moreover, we define D_j as the sum of w and d_j (j=1, 2, 3), which expression is given as follows.

$$D_1 = w + d_1, D_2 = w + d_2, D_3 = w + d_3. \tag{6}$$

The refractive indexes of silicon dioxide and silicon are set as 1.45 and 3.5, respectively. For gold-material, the permittivity at high frequency is described by revised Drude model[23] as follows

$$\varepsilon(w) = \varepsilon_\infty - \frac{w_p^2}{w^2 + i\gamma w}, \tag{7}$$

where the real part

$$\varepsilon_{re}(w) = \varepsilon_\infty - \frac{w_p^2}{w^2 + \gamma^2}, \tag{8}$$

and the imaginary part

$$\varepsilon_{im}(w) = \frac{\gamma * w_p^2}{w(w^2 + \gamma^2)}, \tag{9}$$

where the plasma oscillation frequency w_p and the damping coefficient γ are given in[24],ε_∞ is the static electric constant. The refractive index of gold under different wavelengths is given in[25], as shown in Fig. 2. If the angle α of the GNB elements in the middle disk is changed, the azimuth angle φ in Eqs. (1) - (3) is replaced by the expression φ+α.

Preprints (www.preprints.org) | NOT PEER-REVIEWED | Posted: 18 June 2019 doi:10.20944/preprints201906.0168.v1

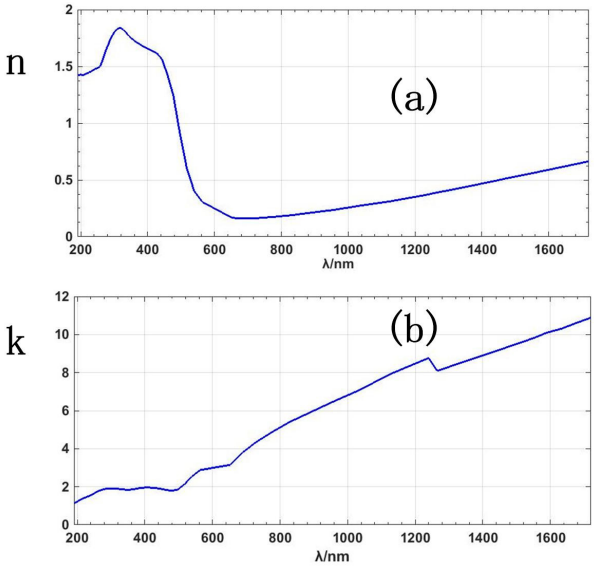

Figure 2. Dependences of the real and imaginary parts of the refractive index of gold on wavelength. Here, n: the real part; k: the imaginary part; λ: wavelength;(**a**): n vs λ; (**b**):k vs λ.

3. Results and discussions

3.1. Far-field radiation

In the following calculations, the transverse magnetic (TM) plane wave with wavelength of 1550nm, as an excitation source, propagates along the direction of the negative z-axis. Its polarization is along the direction of the y-axis, the amplitude of the excitation field is 1 V/m. According to finite element method, the boundary conditions need to be set for the analysis of the antenna.

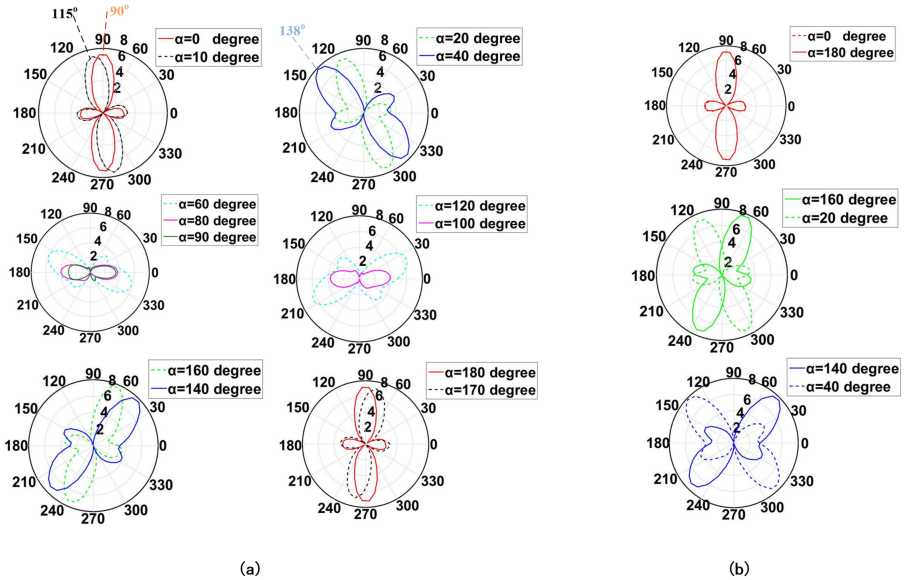

Figure 3. (**a**): Evolutions of the pattern in the xoy-plane of the plasmon nano-optical antenna with the angle α under λ=1550nm; (**b**):Reconfiguration of the pattern in the xoy-plane.

Here, the antenna is surrounded by a spherical shell filled with air and with a radius of 3500nm, which is considered as perfectly matched layer (PML) boundary condition. The thickness of the PML is 800nm. The constants a and b are set as 1069nm, respectively. Fig. 3 shows the evolutions of the pattern in the xoy-plane of the PNOA with the angle α when λ is fixed at 1550nm.It is found from Fig.

Preprints (www.preprints.org) | NOT PEER-REVIEWED | Posted: 18 June 2019 doi:10.20944/preprints201906.0168.v1

3(a) that if α is fixed at a certain value, the pattern in the xoy-plane is symmetrical to the central point. Moreover, the pattern in the xoy-plane can be arbitrarily adjusted by varying α. For example, if α is set as 0°, 10° and 40° in turn, the orientation of the pattern in the xoy-plane, in turn, is 90°, 115° and 138°. One sees further from Fig. 3(b) that the pattern of α is symmetry with that of 180°-α. For example, the pattern α of 20° is symmetry with that α of 160°. This denotes that the pattern can be reconfigured by varying α. Finally, the directivity of the antenna in the xoy-plane becomes worse when α increases from 0° to 90°. However, it will get better with the increase of α from 90° to 180°.

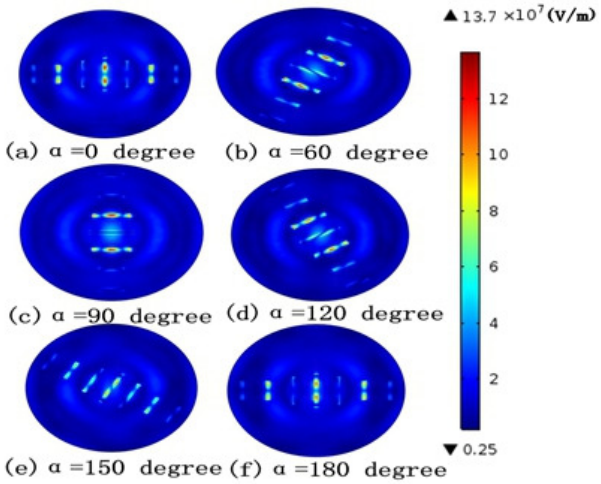

Figure 4. Evolutions of the electric field distribution of the gold nano-block elements with the angle α in the xoy plane at z = 0 nm when λ=1550nm.

To further analyze the reason that the pattern is arbitrarily adjusted, Fig. 4 further gives the evolutions of the electric field distribution for the GNB elements with α in the xoy-plane at z=0 nm when λ is fixed at 1550nm. From Fig. 4, one sees that the positions and numbers of the excited elements are varied with α. For example, if α=0°, the central element with length L_1 and two ones with length L_3, as three bright resonators, are excited strongly. With α fixed at 90°, two ones with length L_2 are excited. When α increases to 150°, all elements are strongly excited.

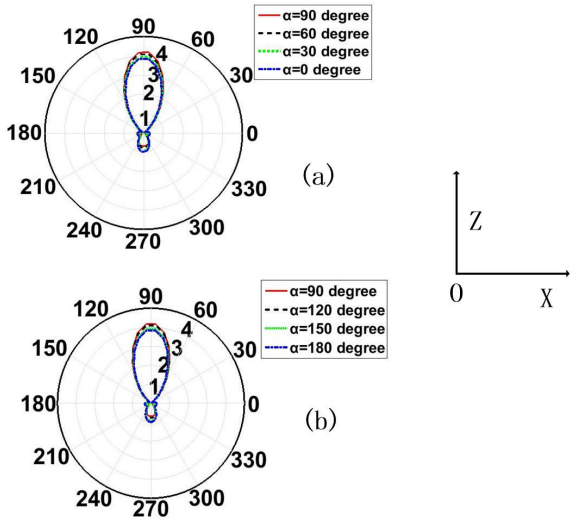

Figure 5. Evolutions of the pattern of the plasmon nano-optical antenna with the angle α in the xoz-plane when λ=1550nm.

As shown in Figs. 5 and 6, the patterns in the xoz and yoz planes are independent of α. But the directivity of the antenna can be slightly changed with α. The reasons are given as follows, according

Preprints (www.preprints.org) | NOT PEER-REVIEWED | Posted: 18 June 2019 doi:10.20944/preprints201906.0168.v1

to traditional antenna theory, if the direction of Yagi antenna structure is adjusted in one plane, the energy radiation direction in the plane will be changed, but that in the other plane can be unchanged.

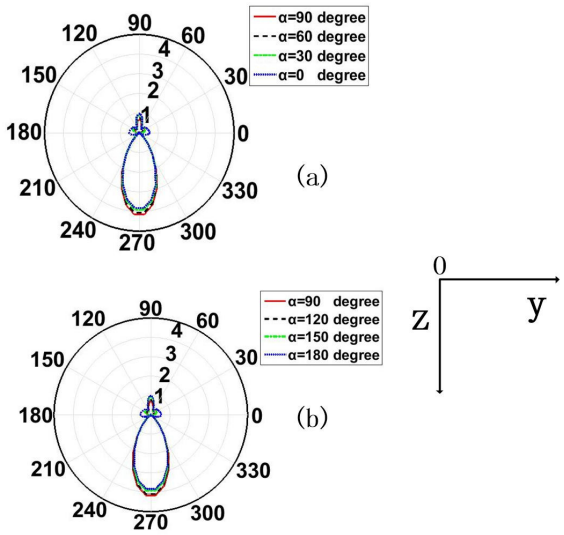

Figure 6. Evolutions of the pattern of the plasmon nano-optical antenna with the angle α in the yoz-plane when λ=1550nm.

3.2. Far-field radiation

The property of the near-field transmission is described by the transmittance, which depends on the S-parameters. Here, the S-parameters, as scattering parameters, originate from transmission-line theory and defined as the ratio of the voltage of transmitted wave and that of reflected waves. But for high-frequency wave, since voltage is not easy to be defined, it is necessary that S-parameters is defined as a function of electric field when the port is excited by fundamental eigenmode. The amplitude E_p of the computed electric field on the port consists of the excitation and reflection fields. On the boundary of the port with an incident wave, E_p is written as

$$E_p = E_0 + \sum_{i=1} S_{i1} E_i, \tag{10}$$

where E_0 is the amplitude of the excitation field; E_i is the amplitude of the ith reflected mode filed. On the boundaries of the other ports, the computed field E_p is expressed by

$$E_p = \sum_{i=1} S_{i1} E_i. \tag{11}$$

Here, the PNOA are considered as two ports (see Fig. 7), where there are two reflected mode fields. Namely, i=1, 2. Therefore, the S-parameters are defined as

$$S_{11} = \frac{\int\limits_{port1} (E_p - E_1) E_1^* \, dA_1}{\int\limits_{port1} E_1 E_1^* \, dA_1}, \tag{12}$$

$$S_{21} = \frac{\int\limits_{port2} (E_p - E_2) E_2^* \, dA_2}{\int\limits_{port2} E_2 E_2^* \, dA_2}, \tag{13}$$

 doi:10.20944/preprints201906.0168.v1

where S_{11} is the reflection coefficient at port 1; S_{21} is the transmission coefficient from port 1 to port 2; A_1 and A_2 are the cross-section area of the port 1 and that of the port 2, respectively. So, we obtain the transmittance as follows.

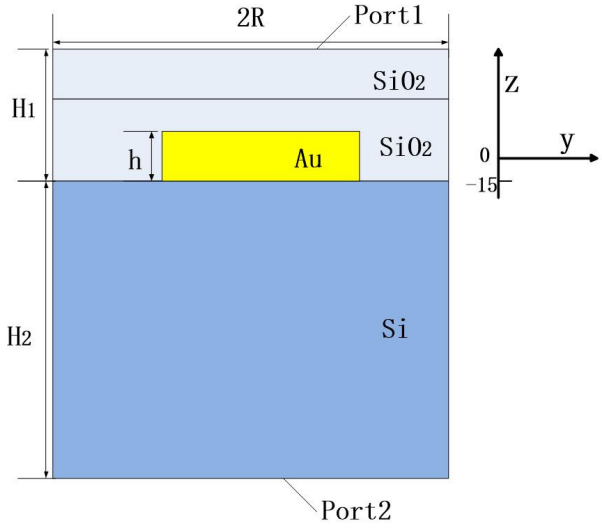

Figure 7. Side view of the plasmon nano-optical antenna.

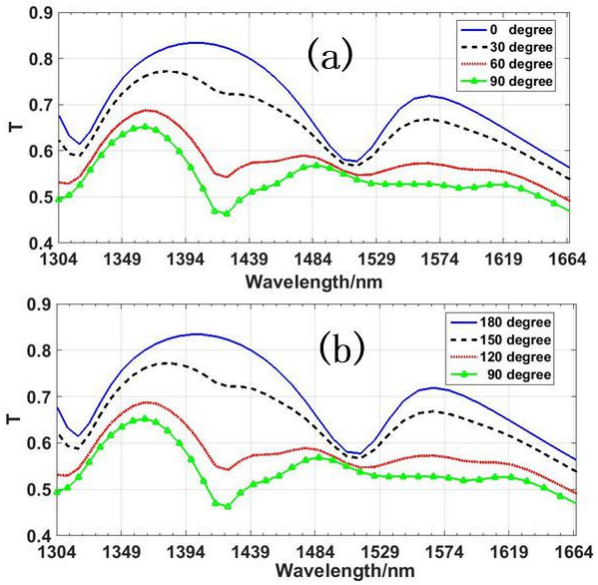

Figure 8. Dependence of the transmissivity on the operating wavelength under different angle α.

Preprints (www.preprints.org) | NOT PEER-REVIEWED | Posted: 18 June 2019 doi:10.20944/preprints201906.0168.v1

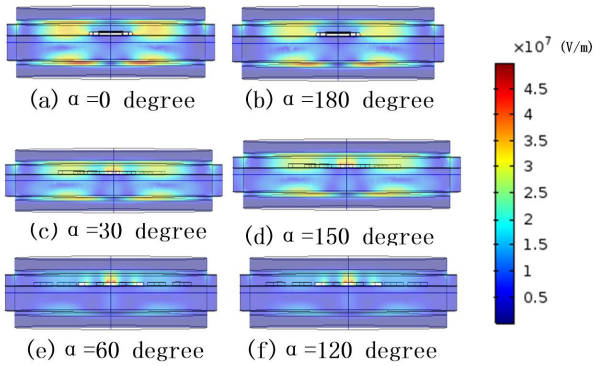

Figure 9. Evolutions of the electric field distribution in the yoz-plane at x = 0 nm with the angle α under λ=1550nm.

$$T = |S_{21}|^2. \tag{14}$$

For convenience of discussion, H_3 is considered as 0 nm (see Fig. 7). Fig. 8 shows the dependences of the transmissivities on the operating wavelength in near infrared band under different α when b_0=1000nm, b_1=1069nm and w=100nm. From Fig. 8, one sees that two transmission peaks occur at 1550nm and 1428.5nm, respectively. One transmission valley appears at 1515.1nm when α=0°. With the increase of α from 0° to 90°, the transmissivity is further decreased and the transmission spectrum gradually become flat. When α further increases from 90° to 180°, the transmission spectrum can be reconfigured. For example, the transmission spectrum under α=30° is the same as that under α= 150°. To clearly explore the effect of α on the transmissivity, Fig. 9 further displays the evolutions of the electric field distribution with α in the yoz-plane at x=0 nm when λ=1550nm. As shown in Fig. 9, the electric field distribution at α=0°, 30° and 60°, in turn, is the same as that at α=180°, 150° and 120°, indicating that the transmissivity can be reconfigured by controlling α.

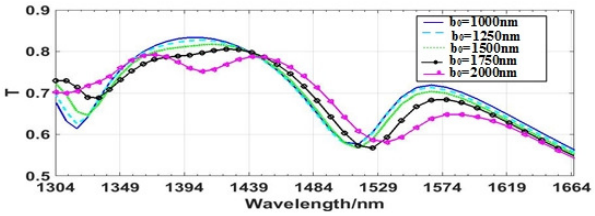

Figure 10. Dependence of the transmissivity on the operating wavelength under different lengths of the elements. Here, d_1=360nm, d_2=d_3=418nm; α=0°; b_1=1069nm; w=100nm; L_1=0.55b_0, L_2=0.45b_0, L_3=0.3b_0 and L_4=0.3b_0.

To observe the influences of the structure of the GNB elements on the transmissivity, Fig. 10 displays the dependences of the transmissivity on the operating wavelength under different lengths of the elements. Here, d_1=360nm, d_2=d_3=418nm; α=0°; b_1=1069nm; w=100nm; L_1=0.55b_0, L_2=0.45b_0, L_3=0.3b_0 and L_4=0.3b_0. As seen from Fig. 10, with the increase of b_0 from 1000 to 2000nm, the transmissivity is gradually decreased in the wavelength range from 1530 to 1666nm. However, in the wavelength range from 1449 to 1515nm, it is further increased. In addition, the transmission spectrums occur red-shift, which may be due to the increase of the resonance wavelength and the enhancement of the resonance strength in the elements (see Fig. 11). Fig. 11 displays the distributions of the electric field in the xoy-plane at z=-15nm under different lengths and the operating wavelengths. It is found from Fig. 11 that the electric fields of the central three elements are further strengthened when the lengths and operating wavelength are increased simultaneously, indicating that the resonance wavelength shifts to longer wavelength.

Preprints (www.preprints.org) | NOT PEER-REVIEWED | Posted: 18 June 2019 doi:10.20944/preprints201906.0168.v1

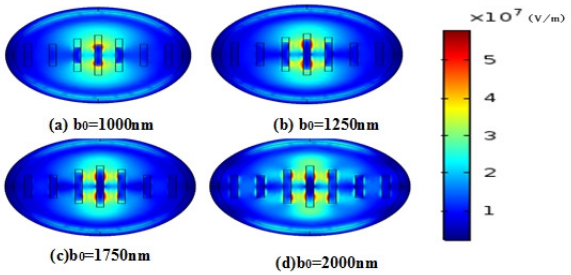

Figure 11. Distributions of the electric field in the xoy-plane at z=-15nm under different lengths of the elements and operating wavelengths. Here, (**a**): b_0=1000nm, λ=1509.4nm; (**b**): b_0=1500nm, λ=1514.2nm; (**c**): b_0=1750nm, λ=1520.5nm (**d**): b_0=2000nm,λ=1533.5nm.

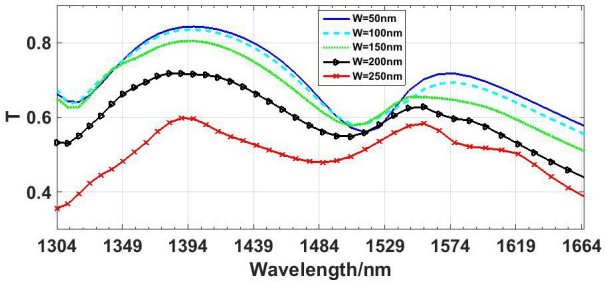

Figure 12. Dependence of the transmissivity on the operating wavelength under different widths of the elements. Here, D_1=280nm, D_2=610nm, D_3=940nm; α=0°; b_0=1000nm; L_1=0.55b_0,L_2=0.45b_0,L_3=0.3b_0 and L_4=0.3b_0.

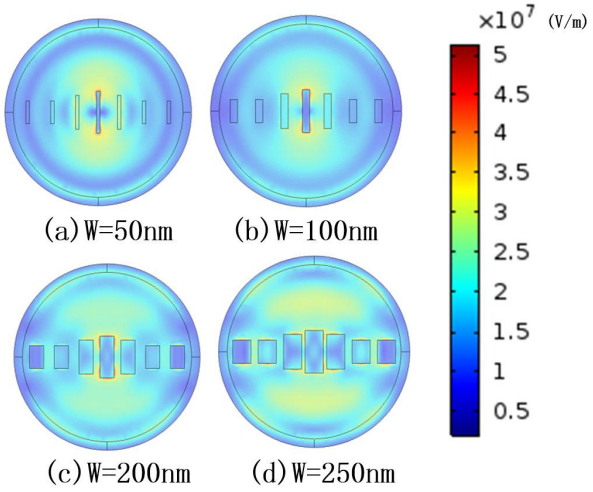

Figure 13. Distributions of the electric field in the xoy-plane at z=-15nm under different widths of the elements and the operating wavelengths. Here (**a**): w=50nm, λ=1518.9nm; (**b**): w=100nm, λ=1509.4nm; (**c**): w=200nm, λ=1500nm; (**d**): w=250nm, λ=1481.4nm.

Figure.12 displays the dependences of the transmissivity on the operating wavelength under different widths of the elements when D_1=280nm, D_2=610nm, D_3=940nm, α=0° and b_0=1000nm. As shown in Fig. 12, with the increase of the width, the transmission valley appears blue-shift. Moreover, the transmissivity is further decreased in the wavelength range of 1428-1500nm and 1530-1664nm, and the peak of side lobe occurs at longer wavelength. The reasons are given as follows: according to Eq. (6), with the increase of the width, the spacings d_1, d_2 and d_3 are further decreased when the D- parameters are fixed different values. Under the condition, as shown in Fig. 13, the interaction

between two elements is gradually enhanced, which induces the generation of side lobe. However, the resonance wavelength is further shortened and the resonance strength is further weakened. These can induce the blue-shift of the transmission valley.

4. Conclusions

A novel PNOA is proposed in this paper. The antenna consists of three vertically superimposed discs with different materials such as silicon and silicon dioxide. Two symmetrical nanometer-scale Yagi antenna elements with gold-material are embedded into the surface of the middle disc. Based on plasmon theory and traditional Yagi antenna theory, the properties of the far-field radiation and near-field transmission in the antenna are further explored. It is found that the pattern in the xoy plane can be arbitrarily adjusted by changing the angle α of the elements in the middle disc. It is noted that the pattern of α is symmetry with that of 180°-α, indicating that the far-field pattern can be reconfigured by varying α. Moreover, the reconfiguration of the near-filed transmission spectrum can be implemented. If α is fixed at 0 degree, the transmission spectrum of optical antenna appears red-shift with the further increase of the lengths of the elements. Finally, the transmission valley occurs blue-shift with the increase of the width of the elements. The antenna proposed in this paper has potential applications some fields such as near-infrared beam scanning plasma devices and multifunctional integrated optical antenna system.

Author Contributions: conceptualization and methodology, D.Z.; software, H.Y.; validation, N.Z., G.Y. and J.Z.; formal analysis,D.Z. and H.Y. ; investigation, G.Y.,J.Z.,N.Z. and H.Y.; writing—original draft preparation, D.Z. and H.Y.; writing—review and editing,N.Z., G.Y. and J.Z.

Funding: This work is supported by the National Natural Science Foundation of China (NSFC) (Grant No. 61475120), and the Major Projects of Basic Research and Applied Research for Natural Science in Guangdong province (Grant No. 2017KZDXM086).

Conflicts of Interest: The authors declare no conflict of interest.

References

1. Romputtal A.;Phongcharoenpanich C . Frequency reconfigurable multiband antenna with embedded biasing network. *Let Microw. Antennas P.* **2017**, *11(10)*, 1369-1378.
2. Morishita A.M.; Gough R.C.; Shiroma W.A.; et al. Liquid-metal frequency-reconfigurable slot antenna using air-bubble actuation.*Electron. Lett* **2015**, *51(21)*, 1630-1632.
3. Lee C.M.; Jung C.W.Radiation-Pattern-Reconfigurable Antenna Using Monopole-Loop for Fitbit Flex Wristband. *IEEE Antennas Wireless Propag. Lett.* **2015**, *14*, 269-272.
4. Alam M.S.; Abbosh A. Planar pattern reconfigurable antenna with eight switchable beams for WiMax and WLAN applications. *Let Microw. Antennas P.* **2016**, *10(10)*, 1030-1035.
5. Yang Z.X.; Yang H.C; Hong J.S.; et al. Bandwidth Enhancement of a Polarization-Reconfigurable Patch Antenna With Stair-Slots on the Ground. *IEEE Antennas Wireless Propag. Letts.* **2014**, *13(5)*, 579-582.
6. Song T.; Woo S.; Park D.; et al. Design of a multipolarization reconfigurable microstrip array antenna using PIN diodes.*Opt. Technol. Lett.* **2013**, *56(1)*, 103-110.
7. Esquius-Morote M.; Gomez-Diaz J.S.; Perruisseau-Carrier J. Sinusoidally Modulated Graphene Leaky-Wave Antenna for Electronic Beamscanning at THz. *IEEE Trans. Terahertz. Sci. Technol.* **2014**, *4(1)*, 116-122.
8. Zhou T.; Cheng Z .; Zhang H.; et al. Miniaturized tunable terahertz antenna based on graphene. *Opt. Technol. Lett.* **2014**, *56(8)*, 1792- 1794.
9. Tatoli T.; Conteduca D.; Dell'Olio, Francesco.; et al. Graphene-based fine-tunable optical delay line for optical beamforming in phased-array antennas. *Appl. Opt.* **2016**, *55(16)*, 4342-4349.
10. Wu Y.; Qu M.; Jiao L.; et al. Graphene-based Yagi-Uda antenna with reconfigurable radiation patterns. *AIP Adv.* **2016**, *6(6)*, 119-135.
11. Bharadwaj P.; Deutsch B .;Novotny L . Optical Antennas.*Adv. Opt. Photonics.* **2009**, *1(3)*, 438-483.
12. Greffet J.J. Nanoantennas for Light Emission. *Science* **2015**, *308(5728)*, 1561-1563.
13. Taminiau T.H.; Stefani F.D.; Segerink F.B.; et al. Optical antennas direct single-molecule emission. *Nat. Photon.* **2008**, *2(4)*,234-237.

14. Gao S.; Ueno K.; Misawa H. Plasmonic Antenna Effects on Photochemical Reactions. *Acc. Chem. Res.* **2011**, *44(4)*, 251-260.
15. Won, Rachel. Surface plasmons: Optical antennas for sensing. *Nat. Photon.* **2007**, *1(8)*, 442-442. .
16. Buret M.; Uskov A.V.; Dellinger J.; et al. Spontaneous Hot-Electron Light Emission from Electron-Fed Optical Antennas. *Nano Lett.* **2015**, *15(9)*, 5811-5818.
17. Appavoo K.; Lei D.Y.; Sonnefraud Y.;et al. Role of Defects in the Phase Transition of VO2 Nanoparticles Probed by Plasmon Resonance Spectroscopy. *Nano Lett* **2012**, *12(2)*, 780-786.
18. Zhang W.; Martin O.J.F.A Universal Law for Plasmon Resonance Shift in Biosensing. *ACS Photon.* **2015**, *2(1)*, 144-150.
19. Munárriz J.; Malyshev A.V.; Malyshev V. A.; Malyshev J. Knoester. Optical nanoantennas with tunable radiation patterns. *Nano Lett.* **2013**, *13(2)*, 444-450.
20. Chen K.; Razinskas G.; Feichtner T.; et al. Electromechanically Tunable Suspended Optical Nano-antenna. *Nano Lett.* **2016**, *16(4)*, 2680-2685.
21. Lalisse A .; Tessier G .;Plain, Jérome.; et al. Plasmonic efficiencies of nanoparticles made of metal nitrides (TiN, ZrN) compared with gold. **2016**, *6(38647)*, 1-10.
22. Hofmann H.F.; Kosako T.; Kadoya Y . Design parameters for a nano-optical Yagi–Uda antenna. *New J. Phys.* **2007**, *9(7)*, 217-230.
23. Johnson P.B.; Christy R.W . Optical Constants of the Noble Metals.*Phys. Rev. B.* **1972**, *6(12)*,4370-4379.
24. Lakowicz J.R.Radiative Decay Engineering: Biophysical and Biomedical Applications. *Anal. Biochem.* **2001**, *298(1)*, 1-24.
25. Palik E.D. Handbook of optical constants of solids II.*Optica Acta International Journal of Optics.* **1991**, *39(1)*,1-1054.